Inorg. Chem. **2005**, *44*, 8723–8732

Cationic Bis-cyclometalated Iridium(III) Diimine Complexes and Their Use in Efficient Blue, Green, and Red Electroluminescent Devices

Arnold B. Tamayo, Simona Garon, Tissa Sajoto, Peter I. Djurovich, Irina M. Tsyba, Robert Bau, and Mark E. Thompson*

Department of Chemistry, University of Southern California, Los Angeles, California 90089

Received June 15, 2005

A series of cationic Ir(III) complexes with the general formula $(C^{\wedge}N)_2Ir(N^{\wedge}N)^+PF_6^-$ featuring bis-cyclometalated 1-phenylpyrazolyl-*N*,$C^{2'}$ ($C^{\wedge}N$) and neutral diimine ($N^{\wedge}N$, e.g., 2,2′-bipyridyl) ligands were synthesized and their electrochemical, photophysical, and electroluminescent properties studied. Density functional theory calculations indicate that the highest occupied molecular orbital of the compounds is comprised of a mixture of Ir d and phenylpyrazolyl-based orbitals, while the lowest unoccupied molecular orbital has predominantly diimine character. The oxidation and reduction potentials of the complexes can be independently varied by systematic modification of either the $C^{\wedge}N$ or $N^{\wedge}N$ ligands with donor or acceptor substituents. The electrochemical redox gaps ($E_{ox} - E_{red}$) were adjusted to span a range between 2.39 and 3.08 V. All of the compounds have intense absorption bands in the UV region assigned to $^1(\pi-\pi^*)$ transitions and weaker charge-transfer (CT) transitions that extend to the visible region. The complexes display intense luminescence both in fluid solution and as neat solids at 298 K that is assigned to emission from a triplet metal–ligand-to-ligand CT (^{3}MLLCT) excited state. The energy of the ^{3}MLLCT state varies in nearly direct proportion to the size of the electrochemical redox gap, which leads to emission colors that vary from red to blue. Three of the $(C^{\wedge}N)_2Ir(N^{\wedge}N)^+PF_6^-$ complexes were used as active materials in single-layer light-emitting electrochemical cells (LECs). Single-layer electroluminescent devices were fabricated by spin-coating the Ir complexes onto an ITO–PEDOT/PSS substrate followed by deposition of aluminum contacts onto the organic film. Devices were prepared that give blue, green, and red electroluminescence spectra (λ_{max} = 492, 542, and 635 nm, respectively), which are nearly identical with the photoluminescence spectra of thin films of the same materials. The single-layer LECs give peak external quantum efficiencies of 4.7, 6.9, and 7.4% for the blue, green, and red emissive devices, respectively.

Introduction

Light-emitting electrochemical cells (LECs) offer a number of advantages over traditional organic light-emitting diodes (OLEDs). Typical OLEDs require a multilayered structure for charge injection, transport, and light emission, as well as a low-work-function metal cathode and a high-work-function metal or metal oxide anode to provide efficient charge injection.[1−4] LECs require only a single layer of organic semiconductor, which is processed directly from solution. LECs generally give low turn-on voltages, close to the photon energy, which are largely independent of the thickness of the active layer. Furthermore, charge injection in an LEC is insensitive to the work function of the electrode material, thus permitting the use of a wide variety of metals as cathode materials, including those with moderate to high work functions, such as gold.[5−7]

The first example of a solid-state LEC was demonstrated by Pei et al.[8] The LEC was based on a spin-cast polymer blend sandwiched between two electrodes. The polymer blend was comprised of a mixture of a semiconducting and

* To whom correspondence should be addressed. E-mail: met@usc.edu.

(1) Tang, C. W.; Van Slyke, S. A. *Appl. Phys. Lett.* **1987**, *51*, 913−915.
(2) Parker, I. D. *J. Appl. Phys.* **1994**, *75*, 1656−1666.
(3) Hughes, G.; Bryce, M. R. *J. Mater. Chem.* **2005**, *15* (1), 94−107.
(4) Forrest, S. R. *Nature* **2004**, *428*, 911−918.
(5) Armstrong, N. R.; Wightman, R. M.; Gross, E. M. *Annu. Rev. Phys. Chem.* **2001**, *52*, 391−422.
(6) Edman, L.; Summers, M. A.; Buratto, S. K.; Heeger, A. *J. Phys. Rev. B* **2004**, *70*, 115212−115217.
(7) Slinker, J.; Bernards, D.; Houston, P. L.; Abruña, H. D.; Bernhard, S.; Malliaras, G. G. *Chem. Commun.* **2003**, 2392−2399.
(8) (a) Pei, Q.; Yu, G.; Zhang, C.; Yang, Y.; Heeger, A. J. *Science* **1995**, *269*, 1086−1088. (b) Pei, Q.; Yu, G.; Zhang, C.; Yang, Y.; Heeger, A. J. *J. Am. Chem. Soc.* **1996**, *118*, 3922−3929.

10.1021/ic050970t CCC: $30.25
Published on Web 11/03/2005

luminescent polymer (MEH/PPV), a salt ($Li^+CF_3SO_3^-$), and an ion-conducting polymer [poly(ethylene oxide), PEO] in which the salt dissolves. When an external bias is applied, the polymer is oxidized (p-type doping) at the anode and reduced at the cathode (n-type doping). Ions redistribute within the organic film to compensate for the charge buildup due to polymer doping. Li^+ ions concentrate near the cathode and $CF_3SO_3^-$ near the anode. This ion redistribution leads to a significant delay between the time a bias is applied and light emission is observed because electron−hole recombination occurs at the newly formed p−n junction. This process is reversible, such that when the bias is removed, the p and n dopings are lost and the ions return to a homogeneous distribution within the film. The function of the PEO is to facilitate the transport of charge-compensating ions to the p- and n-doped regions. Luminance values of 200 cd m^{-2} at 4 V and external quantum efficiencies (EQEs) as high as 2% have been reported for this system.[8−10]

Recently, it has been demonstrated that cationic chelated complexes containing $4d^6$ and $5d^6$ metal ions, e.g., Ru^{2+} and Os^{2+}, can be used as active materials in solid-state LECs[11−14] and have several advantages over the polymer-based LECs. These metal complexes can be synthesized and purified with relative ease (compared to semiconducting polymers). They show excellent electrochemical, photochemical, and thermal stability, good charge-transport properties, long-lived excited states, and good photoluminescence (PL) efficiencies. The positive charges on the complexes are compensated for by negatively charged counterions (e.g., PF_6^- or ClO_4^-). Thus, LECs based on charged metal complexes do not require the presence of an added electrolyte or an ion-conducting polymer, making the device architecture simpler than that of polymer-based LECs. Similar to the situation for polymer-based LECs, the anions migrate into the p-doped region; however, the n-doping process involves reduction of the metal complex, so cation migration into the n-doped region is not required. This simplified redistribution process results in a short turn-on time in these devices, which ranges from several seconds to minutes.[7,11−14]

Most of the single-layer electroluminescent devices based on transition-metal complexes have employed bipyridyl complexes of Ru(II) and Os(II). While devices fabricated using these metal complexes have reached EQEs of 5.5%[11c] and 1.1%,[14] respectively, only orange−red emission has been reported thus far. Recently, charged complexes containing the bis-cyclometalated Ir(III) moiety have been found to be more versatile in terms of color tunability[15−17] and device efficiency.[18,19] The cationic complexes that were examined in LECs have been limited to those with a phenylpyridine-based cyclometalating ligand, e.g., $(ppy)_2Ir(bpy)^+$ [ppy = 2-phenylpyridinato-*N*,*C*$^{2'}$; bpy = 2,2′-bipyridine]. However, there is some ambiguity concerning the nature of the lowest excited state in these complexes because emission can occur from triplet states localized on either the ppy or bpy ligands.[20] The uncertainty comes about from the fact that the triplet energies of phenylpyridyl and bipyridyl ligands are nearly identical (ppy, $^3\pi-\pi^* = 430$ nm; bpy, $^3\pi-\pi^* = 436$ nm).[21] Replacing ppy with a higher energy *C*^*N* ligand such as 1-phenylpyrazolyl (ppz, $^3\pi-\pi^* = 380$ nm)[22] simplifies spectral characterization, such that the lowest triplet state can be unambiguously assigned to the "Ir(bpy)" fragment of $(ppz)_2Ir(bpy)^+$. Cyclometalated compounds of Ir-containing ppz are known to have emission energies higher than those of ppy-based derivatives.[23−25] To date, however, a systematic study on the effect that changes in the ppz or bpy ligands have on the electrochemical and photophysical properties of these compounds has not been reported, nor has their use as emissive materials been demonstrated in electroluminescent devices.

In this paper, we report on the synthesis and photophysical characterization of a series of luminescent $(C^{\wedge}N)_2Ir(N^{\wedge}N)^+$ compounds containing ppz-based cyclometalating ligands. We demonstrate the ability to tune the emission color by varying the electrochemical gap of the parent compound, $(ppz)_2Ir(bpy)^+PF_6^-$, which emits yellow−green. Blue emis-

(9) Pei, Q.; Yang, Y.; Yu, G.; Cao, Y.; Heeger, A. J. *Synth. Met.* **1997**, *85*, 1229−1232.
(10) Pei, Q.; Yang, Y. *Synth. Met.* **1996**, *80*, 131−136.
(11) (a) Lee, J.; Yoo, D.; Rubner, M. F. *Chem. Mater.* **1997**, *9*, 1710−1712. (b) Handy, E. S.; Pal, A. J.; Rubner, M. F. *J. Am. Chem. Soc.* **1999**, *121*, 3525−3528. (c) Rudmann, H.; Shimada, S.; Rubner, M. F. *J. Am Chem. Soc.* **2002**, *124*, 4918−4921. (d) Takane, N.; Gaynor, W.; Rubner, M. F. *Polym. Prepr. (Am. Chem. Soc., Div. Polym. Chem.)* **2004**, *45*, 349. (e) Rudmann, H.; Shimada, S.; Rubner, M. F. *J. Appl. Phys.* **2003**, *94* (1), 115−122. (f) Rudmann, H.; Rubner, M. F. *J. Appl. Phys.* **2001**, *90*, 4338−4345. (g) Rudmann, H.; Shimada, S.; Rubner, M. F.; Oblas, D. W.; Whitten, J. E. *J. Appl. Phys.* **2002**, *92*, 1576−1581.
(12) (a) Kalyuzhny, G.; Buda, M.; McNeill, J.; Barbara, P.; Bard, A. J. *J. Am. Chem. Soc.* **2003**, *125*, 6272−6283. (b) Gao, F. G.; Bard, A. *J. Chem. Mater.* **2002**, *14*, 3465−3470. (c) Buda, M.; Kalyuzhny, G.; Bard, A. J. *J. Am. Chem. Soc.* **2002**, *124*, 6090−6098. (d) Gao, F. G.; Bard, A. J. *J. Am. Chem. Soc.* **2000**, *122*, 7426−7427. (e) Fan, F. F.; Bard, A. J. *J. Phys. Chem. B* **2003**, *107*, 1781−1787. (f) Liu, C.; Bard, A. J. *J. Am. Chem. Soc.* **2002**, *124*, 4190−4191.
(13) (a) Bernhard, S.; Barron, J. A.; Houston, P. L.; Abruña, H. D.; Ruglovsky, J. L.; Gao, X.; Malliaras, G. G. *J. Am. Chem. Soc.* **2002**, *124*, 13624−13628.
(14) Bernhard, S.; Gao, X.; Malliaras, G. G.; Abruna, H. D. *Adv. Mater.* **2002**, *14* (6), 433−436.
(15) Nazeeruddin, M. K.; Humphry-Baker, R.; Berner, D.; Rivier, S.; Zuppiroli, L.; Graetzel, M. *J. Am. Chem. Soc.* **2003**, *125*, 8790−8797.
(16) Lowry, M. S.; Hudson, W. R.; Pascal, R. A., Jr.; Bernhard, S. *J. Am. Chem. Soc.* **2004**, *126*, 14129−14135.
(17) (a) Lo, K. K.; Chung, C.; Lee, T. K.; Lui, L.; Tsing, K. H.; Zhu, N. *Inorg. Chem.* **2003**, *42*, 6886. (b) Lo, K. K.; Chan, J. S.; Chung, C.; Lui, L. *Organometallics* **2004**, *23*, 3108−3116. (c) Lepeltier, M.; Lee, T. K.; Lo, K. K.; Toupet, L.; Le Bozec, H.; Guerchais, V. *Eur. J. Inorg. Chem.* **2005**, 110−117.
(18) Slinker, J.; Koh, C. Y.; Malliaras, G. G. *Appl. Phys. Lett.* **2005**, *8*, 1735061−1735063.
(19) Slinker, J. D.; Gorodetsky, A. A.; Lowry, M. S.; Wang, J.; Parker, S.; Rohl, R.; Bernhard, S.; Malliaras, G. G. *J. Am. Chem. Soc.* **2004**, *126*, 2763−2767.
(20) (a) Columbo, M. G.; Güdel, H. U. *Top. Curr. Chem.* **1994**, *171*, 143−171. (b) King, J. A.; Watts, R. J. *J. Am. Chem. Soc.* **1987**, *109*, 1589−1590. (c) Garces, F. O.; King, J. A.; Watts, R. J. *Inorg. Chem.* **1988**, *27*, 3464−3471.
(21) Maestri, M.; Sandrini, D.; Balzani, V.; Maeder, U.; von Zelewsky, A. *Inorg. Chem.* **1987**, *26*, 1323−1327.
(22) Pavlik, J. W.; Connors, R. E.; Burns, D. S.; Kurzwell, E. M. *J. Am. Chem. Soc.* **1993**, *115*, 7645−7652.
(23) Tamayo, A. B.; Alleyne, B. D.; Djurovich, P. I.; Lamansky, S.; Tsyba, I.; Ho, N. N.; Bau, R.; Thompson, M. E. *J. Am. Chem. Soc.* **2003**, *125*, 7377−87.
(24) Dedeian, K.; Shi, J.; Nigel, S.; Forsythe, E.; Morton, D. *Inorg. Chem.* **2005**, *44*, 4445−4447.
(25) Lo, K. K.; Chan, J. S.; Chung, C.; Tsang, V. W.; Zhu, N. *Inorg. Chim. Acta* **2004**, *357*, 3109−3118.

sion is achieved by substituting the 4′ and 6′ positions on the ppz ligand with electron-withdrawing F atoms, while red emission is achieved by changing the diimine ligand from bpy to 2,2′-biquinolyl (biq). We also report on the device characteristics of single-layer electroluminescent devices fabricated using these compounds. The LEC devices cover a larger color gamut and exhibit higher EQEs than values reported for similar single-layer LEC devices made with ruthenium(II) and osmium(II) diimine complexes.

Experimental Section

General Procedures. Solvents and reagents for synthesis were purchased from Aldrich, Matrix Scientific, and EM Science and used without further purification. Acetonitrile (EM Science, anhydrous, 99.8%) and tetra-*n*-butylammonium hexafluorophosphate (TBAH; Fluka, electrochemistry grade) were used for spectroscopic and electrochemical measurements. $IrCl_3 \cdot nH_2O$ was purchased from Next Chimica. The compounds 1-(2′,4′-difluorophenyl)pyrazole, 1-(4′-*tert*-butylphenyl)pyrazole, and 1-(5′-methoxyphenyl)pyrazole were prepared following literature procedures.[26] All experiments involving $IrCl_3 \cdot nH_2O$ or any other Ir(III) species were carried out in an inert atmosphere despite the stability of the compounds in air, with the main concern being the oxidative and thermal stability of the intermediate complexes at the high temperatures used in the reactions. Cyclometalated Ir(III) dichloro-bridged dimers of the general formula $(C\text{^}N)_2Ir(\mu\text{-}Cl)_2Ir(C\text{^}N)_2$ (where *C*^*N* represents a cyclometalating ligand) were synthesized by the method reported by Nonoyama,[27] which involves the heating of $IrCl_3 \cdot nH_2O$ with 2−2.5 equiv of a cyclometalating ligand in a 3:1 mixture of 2-ethoxyethanol and deionized water to 110 °C.

Synthesis of $(C\text{^}N)_2Ir(N\text{^}N)^+PF_6^-$ Complexes. General Procedure. In a round-bottomed flask, 0.100 g of dichloro-bridged iridium dimer and 2.0 equiv of the diimine are mixed together in 25 mL of methanol. The solution was then refluxed overnight under an inert atmosphere. After cooling to room temperature, counterion exchange from Cl^- to PF_6^- was accomplished via a metathesis reaction in which complexes **1**−**9** were precipitated from the methanol solution with an excess of NH_4PF_6, washed with water and methanol, and dried.

(i) Iridium(III) Bis[1′-phenylpyrazolato-*N*,*C*$^{2'}$]-2,2′-bipyridine Hexafluorophosphate (1). Yield: 83.2%. ^{1}H NMR (360 MHz, CD_2Cl_2): δ 8.49 (d, J = 8.1 Hz, 2H), 8.19 (dd, J = 5.4 and 1.5 Hz, 2H), 8.17 (d, J = 2.7 Hz, 2H), 8.15 (ddd, J = 8.1, 8.1, and 1.7 Hz, 2H), 7.48 (ddd, J = 8.1, 5.4, and 1.0 Hz, 2H), 7.36 (dd, J = 8.1 and 1.2 Hz, 2H), 7.09 (ddd, J = 7.6, 7.3, and 1.2 Hz, 2H), 6.9 (dt, J = 7.8, 7.8, and 1.5 Hz, 2H), 6.87 (dt, J = 2.2 Hz, 2H), 6.56 (dd, J = 3.2 and 2.4 Hz, 2H), 6.33 (dd, J = 7.3 and 1.2 Hz, 2H). ^{13}C NMR (90.55 MHz, CD_2Cl_2): δ 156.8, 151.6, 143.3, 140.0, 138.5, 133.7, 132.2, 128.3, 127.6, 127.4 124.7, 123.9, 112.9, 108.7. Anal. Calcd for $C_{28}H_{22}F_6IrN_6P$: C, 43.13; H, 2.84; N, 10.78. Found: C, 42.86; H, 2.55; N, 10.34.

(ii) Iridium(III) Bis[1′-phenylpyrazolato-*N*,*C*$^{2'}$]-4,4′-di-*tert*-butyl-2,2′-bipyridine Hexafluorophosphate (2). Yield: 78.5%. ^{1}H NMR (360 MHz, CD_3CN): δ 8.32 (d, J = 2.9 Hz, 2H), 8.05 (d, J = 2.9 Hz, 2H), 7.97 (d, J = 5.9 Hz, 2H), 7.38 (dd, J = 5.6 and 1.2 Hz, 2H), 7.01 (dd, J = 8.8 and 7.8 Hz, 2H), 6.94 (d, J = 2.2 Hz, 2H), 6.83 (dd, J = 8.1 and 7.6 Hz, 2H), 6.54 (dd, J = 2.9 and 2.44 Hz, 2H), 6.29 (d, J = 7.6 Hz, 2H), 1.42 (s, 18H). ^{13}C NMR (90.55 MHz, CD_3CN): δ 165.1, 157.2, 151.4, 144.2, 139.3, 134.0, 133.7, 128.8, 127.5, 125.8, 124.1, 122.6, 112.8, 109.6, 36.5, 30.5. Anal. Calcd for $C_{36}H_{38}F_6IrN_6P$: C, 48.48; H, 4.29; N, 9.42. Found: C, 48.48; H, 4.29; N, 9.06.

(iii) Iridium(III) Bis[1′-phenylpyrazolato-*N*,*C*$^{2'}$]-4,4′-dimethoxy-2,2′-bipyridine Hexafluorophosphate (3). Yield: 90.2%. ^{1}H NMR (360 MHz, CD_3CN): δ 7.80 (dd, J = 3.1 and 0.4 Hz, 2H), 7.42 (d, J = 2.89 Hz, 2H), 7.32 (d, J = 8.0 and 1.2 Hz, 2H), 6.44−6.55 (m, 6H), 6.30 (ddd, J = 7.8, 7.3, and 1.2 Hz, 2H), 6.03 (dd, J = 2.8 and 2.3 Hz, 2H) 5.72 (dd, J = 7.5 and 1.4 Hz, 2H), 3.45 (s, 6H). ^{13}C NMR (90.55 MHz, CD_3CN): δ 168.9, 158.9, 152.8, 144.4, 139.4, 134.1, 133.6, 128.8, 127.5, 124.0, 114.4, 112.9, 112.1, 109.1, 57.7. Anal. Calcd for $C_{30}H_{26}F_6IrN_6O_2P$: C, 42.91; H, 3.12; N, 10.01. Found: C, 43.01; H, 3.08; N, 9.98.

(iv) Iridium(III) Bis[1′-phenylpyrazolato-*N*,*C*$^{2'}$]-4,4′-(dicarboxylic acid diethyl ester)-2,2′-bipyridine Hexafluorophosphate (4). Yield: 85.1%. ^{1}H NMR (360 MHz, CD_3CN): δ 9.04 (s, 2H), 8.35 (d, J = 3.0 Hz, 2H), 8.3 (d, J = 6.7 Hz, 2H), 7.96 (dd, J = 3.9 and 1.5 Hz, 2H), 7.47 (d, J = 8.1 Hz, 2H), 7.08 (dd, J = 8.4 and 7.8 Hz, 2H), 7.01 (d, J = 2.3 Hz, 2H), 6.89 (dd, J = 8.5 and 6.4 Hz, 2H), 6.55 (dd, J = 3.2 and 2.5 Hz, 2H), 6.24 (d, J = 7.4 Hz, 2H), 4.46 (q, J = 7.1 Hz, 4H) 1.41 (dd, J = 7.1 Hz, 6H). ^{13}C NMR (90.55 MHz, $CDCl_3$): δ 162.8, 156.7, 157.7, 142.4, 140.6, 138.7, 133.1, 130.9, 127.5, 127.0, 126.9, 124.0, 123.7, 111.6, 108.7, 63.1, 14.2. Anal. Calcd for $C_{34}H_{30}F_6IrN_6O_4P$: C, 44.20; H, 3.27; N, 9.10. Found: C, 44.16; H, 3.23; N, 9.05.

(v) Iridium(III) Bis[1′-phenylpyrazolato-*N*,*C*$^{2'}$]-2,2′-biquinoline Hexafluorophosphate (5). Yield: 89.0%. ^{1}H NMR (360 MHz, CD_3CN): δ 8.67−8.76 (m, 2H), 8.35 (d, J = 2.9 Hz, 1H), 8.01 (dd, J = 7.8 and 2.9 Hz, 1H), 7.97 (d, J = 8.8 Hz, 2H), 7.58 (ddd, J = 8.3, 6.83, and 0.97 Hz, 1H), 7.38 (dd, J = 7.8 and 0.98 Hz, 2H), 7.26 (ddd, 8.8, 6.8, and 1.66 Hz, 1H), 6.97 (dt, J = 7.81, 7.82, and 0.98 Hz, 1H), 6.96 (d, J = 2.44 Hz, 1H), 6.76 (ddd, J = 7.31, 6.32, and 0.98 Hz, 1H), 6.55 (dd, J = 3.42 and 2.93 Hz, 1H), 6.05 (dd, J = 7.33 and 1.46 Hz, 1H). ^{13}C (90.55 MHz, CD_3CN): δ 160.8, 149.4, 142.0, 140.9, 140.9, 134.0, 132.2, 132.2, 129.9, 129.7, 129.4, 129.2, 129.0, 128.8, 127, 2, 124.1, 122.2, 113.0. Anal. Calcd for $C_{36}H_{26}F_6IrN_6P$: C, 49.15; H, 2.98; N, 9.55. Found: C, 48.95; H, 2.90; N, 9.52.

(vi) Iridium(III) Bis[1′-(4′-*tert*-butylphenyl)pyrazolato-*N*,*C*$^{2'}$]-2,2′-biquinoline Hexafluorophosphate (6). Yield: 93.2%. ^{1}H NMR (360 MHz, $CDCl_3$): δ 8.88 (d, J = 8.8 Hz, 2H), 8.72 (d, J = 8.8 Hz, 2H), 8.06 (d, J = 2.9 Hz, 2H), 7.98 (d, J = 8.8 Hz, 2H), 7.91 (d, J = 8.3 Hz, 2H), 7.50 (dd, J = 8.8 and 7.3 Hz, 2H), 7.16 (ddd, J = 9.3, 6.8, and 1.2 Hz, 2H), 7.09 (d, J = 8.6 Hz, 2H), 6.93 (dd, 8.3 and 2.0 Hz, 2H), 6.75 (d, 2.4 Hz, 2H), 6.52 (dd, J = 2.9 and 2.4 Hz, 2H), 5.92 (d, J = 1.7 Hz, 2H), 1.03 (s, 18H). ^{13}C (90.55 MHz, $CDCl_3$): δ 141.4, 139.5, 139.0, 130.9, 130.4, 129.8, 129.6, 128.7, 128.3, 126.2, 121.9, 119.7, 110.7, 108.3, 34.1, 31.1. Anal. Calcd for $C_{44}H_{42}F_6IrN_6P$: C, 53.27; H, 4.27; N, 8.47. Found: C, 53.05; H, 4.27; N, 8.25.

(vii) Iridium(III) Bis[1′-(5′-methoxyphenyl)pyrazolato-*N*,*C*$^{2'}$]-4,4′-di-*tert*-butyl-2,2′-bipyridine Hexafluorophosphate (7). Yield: 61.3%. ^{1}H NMR (360 MHz, CD_3CN): δ 7.91 (d, J = 1.5 Hz, 2H), 7.81 (d, J = 2.9 Hz, 2H), 7.48 (d, J = 5.9 Hz, 2H), 6.96 (dd, J = 7.3 and 2.0 Hz, 2H), 6.58 (d, J = 2.5 Hz, 2H), 6.38 (d, J = 2.0 Hz, 2H), 6.02 (dd, J = 4.9 and 2.4 Hz, 2H), 6.00 (d, J = 2.4 Hz, 2H), 5.57 (d, J = 8.3 Hz, 2H), 3.22 (s, 6H), 1.44 (s, 18H). ^{13}C NMR (90.55 MHz, $CDCl_3$): δ 164.0, 156.6, 156.3, 150.3, 142.9, 138.3, 133.1, 126.8, 124.7, 121.2, 121.0, 112.5, 108.3, 98.9, 55.5, 35.7, 30.2. Anal. Calcd for $C_{38}H_{42}F_6IrN_6O_2P$: C, 47.94; H, 4.45; N, 8.83. Found: C, 47.6; H, 4.3; N, 8.34.

(26) (a) Finar, I. L.; Rackham, D. M. *J. Chem. Soc. B* **1968**, 211−214. (b) Finar, I. L.; Godfrey, K. E. *J. Chem. Soc.* **1954**, 2293−2298.
(27) Nonoyama, M. *Bull. Chem. Soc. Jpn.* **1974**, *47*, 767−768.

(viii) Iridium(III) Bis[1′-(3′-biphenylyl)pyrazolato-*N*,$C^{2'}$)]-4,4′-di-*tert*-butyl-2,2′-bipyridine Hexafluorophosphate (8). Yield: 91.1%. ^{1}H NMR (360 MHz, CD_3CN): δ 8.51 (d, J = 2.7 Hz, 2H), 8.49 (d, J = 1.7 Hz, 2H), 8.07 (d, J = 5.9 Hz, 2H), 7.78 (d, J = 1.7 Hz, 2H), 7.6 (dd, J = 7.3 and 1.2 Hz, 4H), 7.51 (dd, J = 6.1 and 1.7 Hz, 2H), 7.43 (m, 4H), 7.32 (dt, 7.3 and 1.7 Hz, 2H), 7.05 (d, J = 2.2 Hz, 2H), 6.6 (dd, J = 3.2 and 2.4 Hz, 2H), 6.38 (d, J = 7.6 Hz, 2H), 1.42 (s, 18H). ^{13}C NMR (90.55 MHz, $CDCl_3$): δ 164.0, 156.1, 150.2, 143.4., 140.6, 138.6, 136.5, 128.7, 128.7, 126.9, 126.8, 126.5, 126.5, 125.6 124.9, 120.9, 110.0, 108.6, 35.6, 30.2. Anal. Calcd for $C_{48}H_{46}F_6IrN_6P$: C, 55.22; H, 4.44; N, 8.05. Found: C, 54.92; H, 4.13; N, 7.91.

(ix) Iridium(III) Bis[1′-(4′,6′-difluorophenyl)pyrazolato-*N*,$C^{2'}$]-4,4′-di-*tert*-butyl-2,2′-bipyridine Hexafluorophosphate (9). Yield: 65.6%. ^{1}H NMR (360 MHz, $CDCl_3$): δ 8.40 (d, J = 1.7 Hz, 2H), 8.33 (d, J = 2.7 Hz, 2H), 7.95 (d, J = 5.9 Hz, 2H), 7.46 (dd, J = 5.9 and 1.7 Hz, 2H), 7.01 (d, J = 2.2 Hz, 2H), 6.66 (ddd, J = 12.5, 8.8, and 2.2 Hz, 2H), 6.59 (dd, J = 3.2 and 2.7 Hz, 2H), 5.72 (dd, J = 8.1 and 2.4 Hz, 2H), 1.45 (s, 18H). ^{13}C NMR (90.55 MHz, $CDCl_3$): δ 164.8, 160.3, 156.2, 149.7, 148.9, 138.7, 137.1, 131.4, 131.2, 126.9, 125.2, 121.9, 109.2, 115.1, 109.2, 99.4, 35.8, 30.1. Anal. Calcd for $C_{36}H_{34}F_{10}IrN_6P$: C, 45.86; H, 3.56; N, 8.72. Found: C, 45.62; H, 3.63; N, 8.45.

X-ray Crystallography. Diffraction data for compound **2** ‴were collected at T = 296 K.[2] The data set was collected on a Bruker SMART APEX CCD diffractometer with graphite monochromated Mo Kα radiation (λ = 0.710 73 Å). The cell parameters for the iridium complex were obtained from a least-squares refinement of the spots (from 60 collected frames) using the SMART program. One hemisphere of crystal data for the compound was collected up to a resolution of 0.86 Å, and the intensity data were processed using the Saint Plus program. All of the calculations for the structure determination were carried out using the SHELXTL package (version 5.1).[28] Initial atomic positions were located by Patterson methods using X-ray spectroscopy, and the structure of **2** was refined by a least-squares method using SHELX93 with 17 203 independent reflections within the range of θ = 0.86−27.57°. Absorption corrections were applied by using SADABS.[29] In most cases, hydrogen positions were input and refined in a riding manner along with the attached carbons. A summary of the refinement details and the resulting factors for the complex are given in the Supporting Information.

Density Functional Theory (DFT) Calculations. DFT calculations were performed using the Titan software package (Wavefunction, Inc.) at the B3LYP/LACVP** level. The HOMO (highest occupied molecular orbital) and LUMO (lowest unoccupied molecular orbital) energies were determined using minimized singlet geometries to approximate the ground state. The minimized triplet geometries were used to calculate the triplet molecular orbitals and to approximate the triplet HSOMO (where HSOMO = highest singly occupied molecular orbital) as well as the spin-density surface.

Electrochemical and Photophysical Characterization. Cyclic voltammetry and differential pulse voltammetry were performed using an EG&G potentiostat/galvanostat model 283. Anhydrous acetonitrile was used as the solvent under an inert atmosphere, and 0.1 M TBAH was used as the supporting electrolyte. A glassy carbon rod was used as the working electrode, a platinum wire was used as the counter electrode, and a silver wire was used as a pseudo reference electrode. The redox potentials are based on values measured from differential pulse voltammetry and are reported relative to a ferrocenium/ferrocene (Cp_2Fe^+/Cp_2Fe) redox couple used as an internal reference,[30] while electrochemical reversibility was determined using cyclic voltammetry.

The UV−visible spectra were recorded on a Hewlett-Packard 4853 diode array spectrophotometer. Steady-state emission experiments at room temperature and 77 K were performed on a Photon Technology International QuantaMaster model C-60SE spectrofluorimeter. Phosphorescence lifetime measurements were performed on the same fluorimeter equipped with a microsecond xenoflash lamp or on an IBH Fluorocube lifetime instrument by a time-correlated single-photon counting method using either a 331-, 373-, or 405-nm LED excitation source. Quantum efficiency (QE) measurements were carried out at room temperature in degassed 2-MeTHF solutions using the optically dilute method.[31] Solutions of Coumarin 47 in ethanol (Φ = 0.73)[32] were used as the reference. NMR spectra were recorded on Bruker AM 360-MHz instrument, and chemical shifts were referenced to a residual protiated solvent. Elemental analyses (CHN) were performed at the Microanalysis Laboratory at the University of Illinois, Urbana-Champaign, IL.

Device Fabrication. Prior to device fabrication, indium/tin oxide (ITO) on glass was patterned as 2-mm-wide stripes with a resistivity of 20 $\Omega\ \square^{-1}$. The substrates were cleaned by sonication in a soap solution, rinsed with deionized water, boiled in trichloroethylene, acetone, and ethanol for 5−6 min in each solvent, and dried with nitrogen. Finally, the substrates were treated with UV ozone for 10 min. Poly(3,4-ethylenedioxythiophene)/poly(styrene sulfonate) (PEDOT/PSS), a widely used hole-injecting material, was filtered and spin-coated onto the ITO substrates at a rate of 8000 rpm for 60 s. The substrates were then baked in the oven under vacuum for 40 min at T = 90−100 °C to remove the residual solvent. Films of the iridium complexes were then spin-coated from an acetonitrile solution (30 mg mL^{-1}) onto the cooled substrates. The thicknesses of the films were between 70 and 90 nm, as measured by ellipsometry. Aluminum cathodes (1200 Å) were vapor-deposited onto the substrates in a high-vacuum chamber through a shadow mask that defined four devices per substrate with a 2-mm^2 active area each. The devices were tested within 3 h of device fabrication. The electrical and optical intensity characteristics of the devices were measured with a Keithly 2400 source/meter/2000 multimeter coupled to a Newport 1835-C optical meter, equipped with a UV-818 Si photodetector. Only light emitting from the front face of the device was collected and used in subsequent efficiency calculations. The electroluminescence (EL) spectra were measured on a PTI QuantaMaster model C-60SE spectrofluorimeter, equipped with a 928 PMT detector and corrected for detector response.[33] The emission was found to be uniform throughout the area of each device.

Results and Discussion

Synthesis and Structure. Complexes **1**−**9** (see Figure 1) were synthesized from the dichloro-bridged Ir(III) dimer and

(28) Sheldrich, G. M. *SHELXTL*, version 5.1; Bruker Analytical X-ray System, Inc.: Madison, WI, 1997.
(29) Blessing, R. H. *Acta Crystallogr.* **1995**, *A51*, 33−38.
(30) (a) Gagne, R. R.; Koval, C. A.; Lisenski, G. C. *Inorg. Chem.* **1980**, *19*, 2854−2855. (b) Sawyer, D. T.; Sobkowiak, A.; Roberts, J. L., Jr. *Electrochemistry for Chemists*, 2nd ed.; John Wiley and Sons: New York, 1995; p 467.
(31) (a) Demas, J. N.; Crosby, G. A. *J. Phys. Chem.* **1978**, *82*, 991−1024. (b) Crosby, G. A.; Demas, J. N. *J. Am. Chem. Soc.* **1971**, *93*, 2841−2847. (c) Depriest, J.; Zheng, G. Y.; Goswami, N.; Eichhorn, D. M.; Woods, C.; Rillema, D. P. *Inorg. Chem.* **2000**, *39*, 1955−1963.
(32) Jones, G.; Jackson, W. R.; Choi, C. Y.; Bergmark, W. R. *J. Phys. Chem.* **1985**, *89*, 294−300.
(33) Forrest, S. R.; Bradley, D. D. C.; Thompson, M. E. *Adv. Mater.* **2002**, *15* (13), 1043−1048.

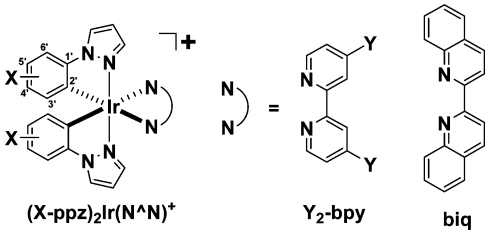

Compound	ppz, X =	N^N, Y =
1	H	bpy, H
2	H	bpy, *t*-butyl
3	H	bpy, OCH_3
4	H	bpy, CO_2Et
5	H	biq
6	5'-*t*-butyl	biq
7	4'-methoxy	bpy, *t*-butyl
8	4'-phenyl	bpy, *t*-butyl
9	4',6'-difluoro	bpy, *t*-butyl

Figure 1. Structure of the $(C^N)_2Ir(N^N)^+PF_6^-$ complexes.

Table 1. Selected Bond Distances and Angles for **2**, *mer*-$Ir(ppz)_3$,[a] and $Ir(bpy)_3^{3+}$ [b]

complex	**2**	*mer*-$Ir(ppz)_3$	$Ir(bpy)_3^{3+}$
Ir−C	2.017(11)	2.057 (2) (cis)	
	2.022(10)	1.993 (2) (trans)	
		2.051 (2) (trans)	
Ir−N	2.005(9) (pz)	2.026(2) (trans)	2.021(6)
	2.015(9) (pz)	2.013(2) (trans)	
	2.140(9), 2.132(9)	2.053 (2)	
N_{pz}−Ir−N_{pz}	173.4(4)	171.54(8)	
C_{pz}−Ir−N_{pz}	80.1(4)	78.57(8)	
	81.3(4)	79.73(8)	
N_{bpy}−Ir−N_{bpy}	76.4(3)		78.7(8)[c]

[a] Reference 23. [b] Reference 34. [c] Average.

2.0 equiv of the diimine ligand in refluxing methanol, followed by metathesis with NH_4PF_6. The complexes were characterized using spectroscopic methods in addition to elemental analysis. ^1H and ^{13}C NMR spectroscopies indicate that the complexes are C_2-symmetric stereoisomers (one set of proton signals for the cyclometalating ligand). The ligand configuration at the Ir(III) center, with cis-metalated phenyl groups and *trans*-pyrazolyl moieties, is illustrated schematically in Figure 1 and confirmed by X-ray crystallography.

Single crystals of complex **2** were grown from an acetone solution and characterized by X-ray crystallography. The crystal data, atomic coordinates, and a complete listing of bond lengths and angles are given in the Supporting Information; selected bond lengths and angles are given in Table 1. A perspective view of the cation is given in Figure 2. For comparison, structural data for the related compounds *mer*-$Ir(ppz)_3$[23] and $Ir(bpy)_3^{3+}$ [34] are also given in Table 1. The C−C and C−N bond lengths and angles are within the normal ranges expected for those of organic fragments. The ligands are arranged in a pseudo-octahedral geometry around the metal center with the expected trans configuration of pyrazolyl groups. The measured bond angle between the *trans*-pyrazolyl groups is 173.4(4)°, comparable to the value

(34) Hazell, A. C.; Hazell, R. G. *Acta Crystallogr.* **1984**, *C40*, 806−811.

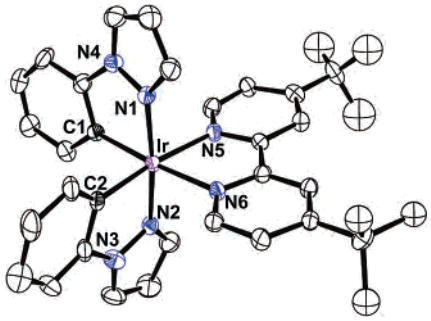

Figure 2. ORTEP drawing of **2**. The thermal ellipsoids for the image represent a 25% probability limit. The hydrogen atoms, counterion, and solvent are omitted for clarity.

of 171.54(8)° reported for *mer*-$Ir(ppz)_3$. The average Ir−C bond length and C_{pz}−Ir−N_{pz} angle are 2.019(11) Å and 80.7(4)°, respectively. These values are also consistent with the values 2.025(2) Å and 79.15(8)° reported for *mer*-$Ir(ppz)_3$. The strong trans influence of the phenyl groups results in slightly longer Ir−N(bpy) bond lengths in **2** [Ir−N_{ave} = 2.136(9) Å] as compared to those of $Ir(bpy)_3^{3+}$, where the average Ir−N bond length is 2.021(6) Å. Likewise, the average N_{pyr}−Ir−N_{pyr} angle for **2** is measured to be 76.4(3)°, comparable to the average value of 78.7(8)° reported for $Ir(bpy)_3^{3+}$.

DFT Calculations. DFT calculations were carried out on all of the complexes at a B3LYP level using a LACVP** basis set to get some insight into the electronic structure of the complexes. A similar approach has been shown to be effective at reproducing the ground- and excited-state properties of related cyclometalated Ir(III) and Pt(II) complexes.[16,35] The discussion here will focus on the results for **1**; however, all of the examined $(C^N)_2Ir(N^N)^+$ complexes gave a similar picture for the HOMO and LUMO surfaces. The calculated Ir−C_{ave} (2.05 Å), Ir−$N_{pz(ave)}$ (2.06 Å), and Ir−N_{pyr} (2.18 Å) bond distances and N_{pz}−Ir−N_{pz} (170.93°), C_{pz}−Ir−N_{pz} (79.56°), and N_{pyr}−Ir−N_{pyr} (75.783°) chelate angles for $(ppz)_2Ir(bpy)^+$ compare favorably to the corresponding experimental values determined in the X-ray structure of **2** as well as to literature values of similar bis-cyclometalated iridium(III) diimine complexes.[25] The singlet HOMO and LUMO and triplet spin-density surfaces of $(ppz)_2Ir(bpy)^+$ are illustrated in Figure 3. The calculated HOMO and LUMO energies for $(ppz)_2Ir(bpy)^+$ in the ground state are −8.01 and −5.10 eV, respectively. The HOMO is principally composed of a mixture of Ir d and phenyl π orbitals distributed equally among the two phenylpyrazolyl ligands, whereas the LUMO is predominantly localized on the bipyridyl ligand. The HOMO and LUMO orbitals are orthogonal to each other, and thus, there is little electronic overlap between them. The orthogonal relationship between the HOMO and LUMO suggests that their energies are amenable to independent variation by simple substitution of either the cyclometalate or the diimine, respectively. The

(35) (a) Hay, P. J. *J. Phys. Chem. A* **2002**, *106*, 1634−1641. (b) Brooks, J.; Babayan, Y.; Lamansky, S.; Djurovich, P. I.; Tsyna, I.; Bau, R.; Thompson, M. E. *Inorg. Chem.* **2002**, *41*, 3055−3066. (c) Zheng, K.; Wang, J.; Shen, Y.; Kung, D.; Yun, F. *J. Phys. Chem. A* **2001**, *105*, 7248−7253.

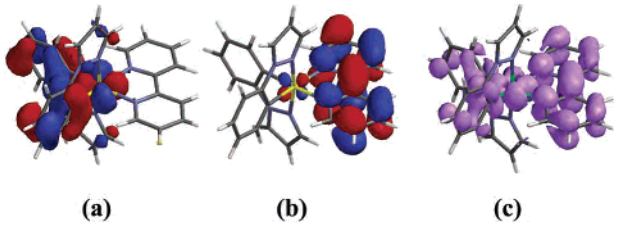

Figure 3. (a) HOMO, (b) LUMO, and (c) triplet spin-density surfaces of $(ppz)_2Ir(bpy)^+$ determined using DFT. The HOMO consists mainly of a mixture of Ir and phenyl π orbitals, while the LUMO has predominantly bipyridyl character.

Table 2. Redox Properties of Compounds **1**−**9**[a]

complex	$E_{1/2}^{ox}$ (V)	$E_{1/2}^{red}$ (V)	$\Delta E_{1/2}$ (V)
1	0.95	−1.80	2.75
2	0.95	−1.89	2.84
3	0.99	−1.90	2.89
4	0.97	−1.42	2.39
5	1.04	−1.36, −1.96	2.40
6	1.01	−1.44, −2.04	2.45
7	0.62	−1.90	2.52
8	0.84	−1.88	2.72
9	1.25	−1.83	3.08

[a] Redox measurements were carried out in an anhydrous CH_3CN solution, and values are reported relative to Fc^+/Fc.

energy calculated for the HSOMO in the geometry-optimized triplet state is −5.50 eV. The difference in energy between the singlet ground-state HOMO and triplet HSOMO was then used to estimate the singlet−triplet transition energy. The calculated transition energy of 2.51 eV (494 nm) is comparable to the energy of the emission band found for $(ppz)_2Ir(bpy)^+$ (487 nm) in 2-MeTHF at 77 K (vide infra). The location of the unpaired spins in the frontier orbitals of the triplet state is illustrated by the spin-density surface (Figure 3c). The spin-density surface shares the same spatial extent as the singlet HOMO and LUMO surfaces, which leads to a description of the lowest energy excited state as having metal−ligand-to-ligand charge-transfer (MLLCT) character. The DFT results will be further used in the text as they pertain to the electrochemical and spectral interpretation.

Electrochemistry. The electrochemical properties of the bis-cyclometalated iridium diimine complexes in acetonitrile were examined using cyclic voltammetry. A summary of the redox potentials, measured relative to an internal ferrocene reference ($Cp_2Fe^+/Cp_2Fe = +0.35$ V vs SCE in acetonitrile), is listed in Table 2. All complexes exhibit reversible oxidation and reduction processes. For example, $(ppz)_2Ir(bpy)^+$ (**1**) has a reversible oxidation wave at 0.95 V and a reversible reduction wave at −1.80 V. For comparison, neutral tris-cyclometalated (ppz)Ir(III) complexes also undergo reversible oxidation at potentials near 0.40 V but are extremely difficult to reduce (reduction potentials < −3.0).[23] The electrochemical gap ($\Delta E_{1/2}^{redox} = E_{1/2}^{ox} - E_{1/2}^{red}$) found for complex **1** (−2.75 V) is similar to the difference in the singlet HOMO and LUMO energies obtained from DFT calculations (−2.91 eV). Therefore, it can be presumed that oxidation is associated with the bis-cyclometalated phenyl-Ir moiety while reduction occurs on the bipyridyl ligand. It follows from the results of the DFT calculations that the oxidation and reduction potentials of the $(C^\wedge N)_2Ir(N^\wedge N)^+$

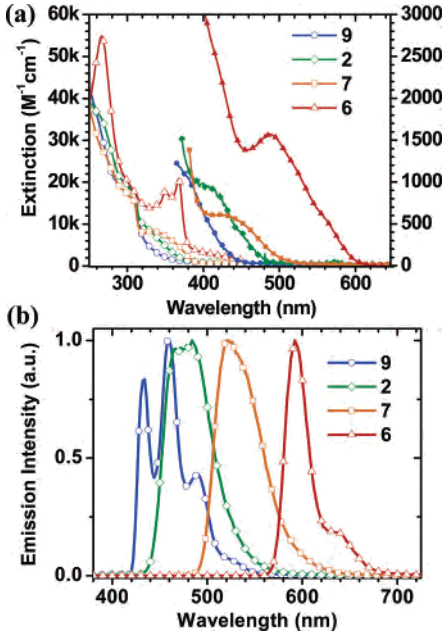

Figure 4. (a) Room-temperature absorption (in CH_3CN) and (b) 77 K emission (in 2-MeTHF) spectra of compounds **2** (◊), **6** (△), **7** (□), and **9** (○). The filled symbols in the absorption spectra correspond to the right axis.

complexes can be independently adjusted by modification of the phenyl and diimine ligands, respectively, with donor or acceptor substituents. For example, complexes **1**−**5**, which differ only by the identity of the diimine ligand, have reduction potentials that vary over 0.53 V (from −1.89 V for **2**, with electron-donating 4,4′-di-*tert*-butyl groups, to −1.36 V for **5,** which has a π-extended 2,2′-biquinolyl ligand). However, the corresponding oxidation potentials differ over a much smaller range, 0.09 V (from 0.95 V for **2** to 1.04 V for **5**). Similarly, complexes **2** and **7**−**9**, each with an identical diimine ligand and modified ppz ligands, have oxidation potentials that vary over 0.63 V (from 0.62 V for **7**, with electron-donating 5′-methoxy substituents, to 1.25 V for **9**, with electron-withdrawing 4′,6′-difluoro substituents), whereas the reduction potentials fall within a narrow range of 0.07 V. The ability to independently adjust the oxidation and reduction potentials of these complexes over a wide range leads to $\Delta E_{1/2}^{redox}$ values that vary from 2.39 V for **4** to 3.08 V for **9**.

Electronic Spectroscopy. Absorption and emission data are summarized in Table 3, while spectra for complexes **2**, **6**, **7**, and **9** are presented in Figure 4a. Spectra for the other complexes are given in the Supporting Information. The absorption spectra of the compounds in acetonitrile show intense bands ($\epsilon > 10^4$ M^{-1} cm^{-1}) in the ultraviolet part of the spectrum between 200 and 300 nm. These bands are assigned to spin-allowed $^1\pi-\pi^*$ ligand-centered (LC) transitions in both $C^\wedge N$ and $N^\wedge N$ ligands. The less intense, lower energy absorption features from 300 to 600 nm are assigned to both spin-allowed and spin-forbidden charge-transfer (CT) transitions. Two types of CT transitions can be distinguished in the spectra, bands between 300 and 400 nm of moderate intensity [$\epsilon \approx (1-2) \times 10^4$ M^{-1} cm^{-1}] and transitions in the visible region with much weaker intensity ($\epsilon \leq 10^3$ M^{-1}

Table 3. Photophysical Properties of Compounds **1**−**9**[a]

complex	absorbance λ (nm) (ϵ, $\times 10^4$ M^{-1} cm^{-1})	emission at room temperature						emission at 77 K	
		λ_{max} (solvent) (nm)	$\tau_{solution}$ (μs)	τ_{powder} (μs)	Φ_{PL}	k_r (10^4 s^{-1})	k_{nr} (10^6 s^{-1})	λ (nm)	τ (μs)
1	216 (5.21), 244 (4.37), 261 (3.81), 298 (1.39) 308 (1.26), 345 (0.97) 436 (0.13)	563 (CH_3CN) 554 (CH_2Cl_2) 565 (2-MeTHF) 550 (neat)	0.48	0.37	0.17	35	2	487	4.8
2	207 (5.70), 248 (3.95), 266 (3.53), 296 (2.04), 308 (1.76), 328 (0.89) 420 (0.09)	555 (CH_3CN) 538 (CH_2Cl_2) 550 (2-MeTHF) 535 (neat)	0.72	0.76	0.076	11	1	465	4.3
3	221 (5.98), 247 (4.50), 267 (3.60), 300 (1.47), 325 (0.92), 417 (0.07)	554 (CH_3CN) 541 (CH_2Cl_2) 550 (2-MeTHF) 532 (neat)	0.53	0.69	0.032	6.0	2	440	6.9
4	212 (5.49), 243 (4.07), 298 (2.10), 325 (1.60), 369 (0.57), 482 (0.10)	628(CH_3CN) 620 (CH_2Cl_2) 625 (2-MeTHF) 615 (neat)	0.10	0.38	0.0012	1.2	10	545	4.4
5	215 (5.48), 258 (6.02), 277 (4.77), 300 (2.23) 323 (1.87), 351 (1.55) 367 (1.88), 417 (0.27) 489 (0.17), 578 (0.06)	616 (CH_3CN) 610 (CH_2Cl_2) 614 (2-MeTHF) 613 (neat)	0.86	0.26	0.017	2.0	1	585	7.7
6	215 (5.39), 266 (5.48), 304 (1.92), 338 (1.44), 350 (1.79), 368 (2.08) 403 (0.32), 426 (0.23) 491 (0.16), 568 (0.05)	627 (CH_3CN) 620 (CH_2Cl_2) 624 (2-MeTHF) 622 (neat)	0.56	0.62	0.0068	1.2	2	592	8.5
7	206 (5.51), 223 (4.85), 244 (3.98), 273 (2.67), 297 (1.82), 307 (1.67) 342 (0.85), 454 (0.05)	618 (CH_3CN) 598 (CH_2Cl_2) 615 (2-MeTHF) 570 (neat)	0.031	0.12	0.0007	2.2	32	522	2.3
8	297 (8.00), 256 (7.81), 297 (3.98), 307 (3.70), 426 (0.09),	570 (CH_3CN) 551 (CH_2Cl_2) 570 (2-MeTHF) 560 (neat)	0.32	0.37	0.010	3.1	3	480	2.4
9	210 (5.72), 246 (4.32), 295 (2.05), 310 (1.68), 386 (0.10)	495 (CH_3CN) 484 (CH_2Cl_2) 493 (2-MeTHF) 487 (neat)	1.34	3.48	0.40	30	0.4	433	3.9

[a] The absorption spectra were measured in CH_3CN. The solution PL efficiencies and lifetimes were measured in degassed 2-MeTHF.

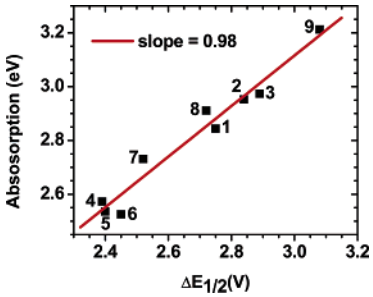

Figure 5. Plot of the absorption energy (in CH_3CN) of lowest CT band vs the redox gap, $\Delta E_{1/2}$, for complexes **1**−**9**.

cm^{-1}). The higher energy bands are assigned to metal-to-ligand CT (MLCT) transitions involving either the cyclometalated or diimine ligand, in analogy to features seen at similar energies in related tris-cyclometalated or diimine Ir complexes.[20,25,36] The lower energy absorption bands are assigned to $(ppz)_2Ir \rightarrow$ diimine MLLCT transitions. There is a direct correlation between the absorption energy of these MLLCT bands and the $\Delta E_{1/2}^{redox}$ values of the respective complexes (Figure 5). The visible absorption bands have low extinction coefficients because of the poor spatial overlap between the molecular orbitals involved in the MLLCT transitions (see Figure 3a,b).[36] The lowest energy absorption shoulders on these bands are assigned to spin-forbidden components of the MLLCT transitions.

The Ir complexes all display broad, featureless emission spectra in a fluid solution or a neat solid at room temperature, with maxima ranging from 485 to 630 nm and luminescence decay lifetimes that fall between 0.031 and 1.34 μs (Table 1). The emission spectra exhibit large Stokes shifts (ca. 4000−6000 cm^{-1}) from the lowest energy absorption bands. The emission properties at room temperature are consistent with luminescence originating from a triplet MLLCT state. The complexes all undergo large rigidochromic blue shifts upon cooling of the solutions to 77 K. For example, the emission maximum of **8** in 2-MeTHF at room temperature is 570 nm, while at 77 K, the maximum is centered at 480 nm. The hypsochromic shifts are due to solvent reorganization in a fluid solution at room temperature, which stabilize the CT states prior to emission. This process is significantly impeded in a rigid matrix at 77 K, and thus emission occurs at higher energy. The emission spectra remain featureless in a 2-MeTHF solution at 77 K except for spectra of complexes **5**, **6**, and **9**, which show a series of vibronic transitions (Figure 4b). The structured emission from com-

(36) Neve, F.; La Deda, M.; Crispini, A.; Bellusci, A.; Puntoriero, F.; Campagna, S. *Organometallics* **2004**, *23*, 5856−5863.

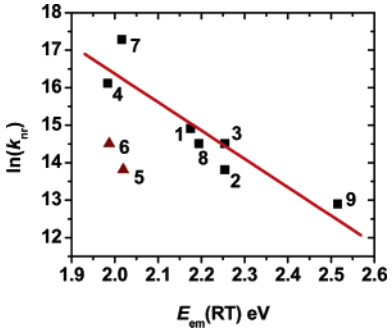

Figure 6. Plot of the nonradiative decay rate [ln(k_{nr})] vs emission energy [E_{em}(RT)] of complexes **1**−**9**. The line shown is the linear fit for complexes with bipyridyl-type ligands.

plexes **5**, **6**, and **9** implies that a considerable LC character develops in these three species at low temperature. In particular, the highly structured emission for complex **9** at 77 K has a highest energy peak (433 nm) that is comparable to what is found for $Ir(bpy)_3^{3+}$ (430 nm),[37] a complex with emission assigned to a ^{3}LC transition. However, the emission lifetime for **9** at 77 K ($\tau = 3.9\ \mu$s) indicates that the MLLCT state still exerts a strong perturbation on the ^{3}LC transition since the value is much shorter than that found for $Ir(bpy)_3^{3+}$ ($\tau = 80\ \mu$s).

The radiative (k_r) and nonradiative (k_{nr}) decay rates calculated from luminescence quantum yield data are given in Table 3. The luminescent quantum yields for the complexes in solution range between 0.0007 for **8** and 0.40 for **9**. The difference in the quantum yields can be attributed to a decline in the nonradiative rates with increasing emission energy because variation in k_{nr} is 10-fold greater than that in k_r. The trend in the nonradiative rates is consistent with energy gap law behavior. The energy gap law states that a series of compounds with similar ground- and excited-state vibrational modes will show a linear correlation between ln(k_{nr}) and the emission energy. A plot ln(k_{nr}) vs emission energy for the $(C\hat{}N)_2Ir(N\hat{}N)^+$ complexes is given in Figure 6. The nonradiative rates for complexes with bipyridyl-type $N\wedge N$ ligands can be linearly correlated with the emission energy, whereas the nonradiative rates for complexes **5** and **6** with biquinolyl ligands are lower than those of complexes with similar emission energies such as **4** and **7**. This difference indicates that the vibrational modes responsible for excited-state deactivation are less effectively coupled to the ground state in the biquinolyl ligands than in the bipyridyl ligands, which leads to more efficient emission from complexes **5** and **6** than from **4** and **7**.

The luminescence properties for neat sample compounds **1**−**9** are also listed in Table 3. The emission spectra for the neat solids are similar to those observed in a CH_2Cl_2 solution at room temperature. The luminescent lifetimes measured for most of the compounds in the solid state are longer than those for samples in degassed solutions. Significant quenching occurs for most of the compounds in a fluid solution. Thus, the luminescent quantum yield of the compounds measured in a solution is not an ideal parameter for evaluating their utility as emissive materials for single-layer electroluminescent devices. However, the lifetimes exhibited by powdered samples of compounds **1** and **5** are shorter than the values in degassed solutions, which indicates that solid-state interactions can lead to significant self-quenching in these species. Increasing the steric bulk of either the bpy or ppz ligands by the addition of *tert*-butyl substituents (i.e., **2** and **6)**, leads to diminished self-quenching, such that the powdered lifetimes for these derivatives are longer than the fluid solution values. This strategy of using bulky alkyl groups to inhibit self-quenching in the solid state has likewise been shown to be effective for $Ru(bpy)_3^{2+}$ complexes, where single-layer LEC devices made with *tert*-butyl-substituted $Ru(bpy)_3^{2+}$ derivatives show improved device performance (Table 4).[11c,13a] Interestingly, the phosphorescent lifetime of **9** in a degassed solution (1.34 μs) is shorter than the value found in the powdered sample (3.5 μs); however, both values are markedly larger than those of compounds **1**−**8**. The τ value for the powdered sample of **9** is similar to the lifetime measured in a solid solution at 77 K. Assuming a quantum yield of near unity at 77 K, the PL quantum yield of **9** in the neat solid at room temperature is also near unity.

Table 4. Summary of Device Data for LECs Prepared with Compounds **2**, **6**, and **9**[a]

compound	λ_{max} (nm)	CIE coordinates	turn-on time[b] (min)	peak EQE (%)	brightness at peak EQE (cd m^{-2})
2	542	$x = 0.37$ $y = 0.59$	35	6.9	11500
6	635	$x = 0.67$ $y = 0.32$	32	7.4	7500
9	492	$y = 0.20$ $y = 0.41$	30	4.6	1700

[a] All devices were run at a constant bias of 3 V. [b] Time required to reach 1.0 cd m^{-2}.

OLED Studies. Blue, green, and red phosphorescent LEC devices were fabricated with compounds **9**, **2**, and **6**, respectively, to test the utility of these Ir complexes in LEC structures. ITO substrates coated with PEDOT/PSS were used to prepare the LECs. The use of PEDOT/PSS is essential for the formation of uniform thin films of the $(C\hat{}N)_2Ir(N\hat{}N)^+PF_6^-$ salt complexes. Films of the Ir(III) salts spin-coated onto bare ITO crystallize rapidly and are prone to the formation of pinholes, whereas PEDOT/PSS-treated substrates give films that have low pinhole densities and appear uniform, even at high magnification (1000×). Thus, the device structure investigated here was ITO−PEDOT/PSS (400 Å)/Ir complex (700−900 Å)/Al (1200 Å). LECs prepared with the three emitters display excellent reproducibility in both their fabrication and electroluminescent behavior. The EL spectra have Commission Internationale de L'Eclairage (CIE) coordinates, which correspond to blue ($x = 0.20$, $y = 0.41$), green−yellow ($x = 0.37$, $y = 0.59$), and red ($x = 0.67$, $y = 0.32$) emission for devices made with complexes **9**, **2**, and **6**, respectively. All three LECs give EL spectra with line widths similar to those of their thin-film PL spectra but show red shifts of 5−10 nm (Figure 7). The EL spectra are independent of the applied voltage and invariant when tested under forward and reverse bias

(37) Flynn, C. M., Jr.; Demas, J. N. *J. Am. Chem. Soc.* **1974**, *96*, 1959−1960.

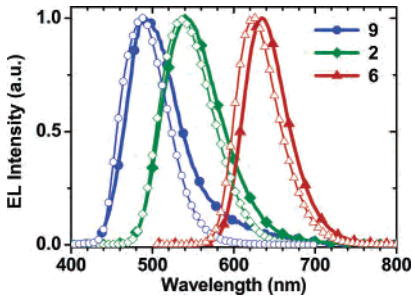

Figure 7. EL and thin-film PL spectra for compounds **2** (◊), **6** (△), and **9** (○). EL spectra are illustrated with solid symbols and PL spectra with open symbols.

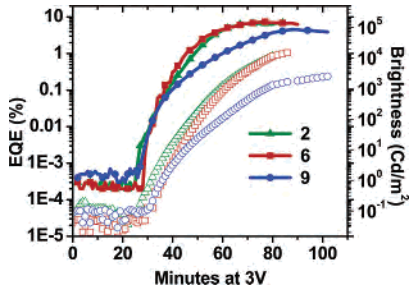

Figure 8. Plot of the light output and device efficiency as a function of time for LECs based on compounds **2** (△), **6** (◊), and **9** (○), held at a constant bias of 3 V. The open symbols show the brightness (cd m^{-2}), and the solid symbols correspond to the EQE (%) values.

(forward is ITO = anode). This behavior is in contrast to the bias-dependent EL spectral shifts reported for LEC devices made with $(ppy)_2Ir(4,4'\text{-di-}tert\text{-butylbipyridine})^+PF_6^-$.[19]

The time dependence of the brightness and QE for each of the three devices is shown in Figure 8. These devices exhibit the characteristic delay in light output observed for LECs and only begin to give visible EL (0.1 cd m^{-2}) after 20−30 min when held at a constant bias of 3 V. The formation of a stable p−n junction by the slow migration of the PF_6^- ions in the thin film toward the anode is responsible for the delay in the LEC response. As the voltage is increased, the delay decreases. For example, at a bias of 5 V, devices show visible emission after only 3−5 min. While this delay in light output is long relative to that of OLEDs, it is shorter than delays reported for other LECs, which can be on the order of hours.[11−14,19] The EQE values for these Ir-based LECs increased steadily after the devices were turned on. The EQE values of LECs made with either complex **2** or **6** take ca. 70 min to reach peak EQE values of 6.9 and 7.4%, respectively, when held at 3 V. In contrast, devices made with the blue emissive complex **9** reach a lower peak EQE of 4.6% after 55 min. The LECs reported here give high power efficiencies. Devices with compounds **2**, **6**, and **9** give peak power efficiencies of 25, 10, and 11 lm W^{-1}, respectively, when biased at 3 V.

Current−voltage (J−V) plots for the LEC using complex **2** were recorded at four different times (Figure 9). The J−V characteristics of the device gradually evolve and ultimately begin to resemble those commonly observed in OLEDs.[38] The initial J−V plot, as well as the one recorded just after

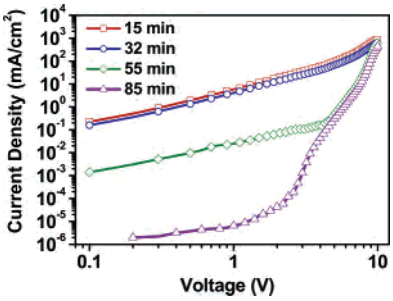

Figure 9. Current−voltage plots measured at different times for an LEC using complex **2**.

emission is observed (15 and 32 min, respectively), shows a high current at low bias that is consistent with a high degree of carrier leakage in the device. This is not surprising because at short operating times the unpolarized device is expected to show a J−V response that is dominated by conduction of a single charge carrier. As the device continues to operate, a p−n junction is formed and the current at low bias decreases significantly. The QE for the device increases as a result of the improved carrier balance. The changes in the current−voltage plots observed for the LEC provide a clear signature of a single-layer device evolving into a single-heterostructure device, in which charge recombination occurs within the organic film, thereby minimizing the losses associated with carrier leakage to either electrode.

The EQE values reported here are some of the highest reported for LEC devices yet still fall short of the values that are common for electrophosphorescent OLEDs (>10%). Because the heterostructure of an LEC device is formed under bias and not in place at the outset of testing, charge recombination is somewhat more complicated than that which occurs in an OLED. Nevertheless, the EQEs should increase with improved carrier balance, and the power efficiencies of LECs could then approach values similar to those of the best p- and n-doped phosphorescent OLEDs.[39]

The reported device lifetimes for LECs have been comparatively short (minutes to hours to half-brightness).[11−13,40,41] Unfortunately, the methods used to evaluate the lifetimes of LECs are not directly comparable to those of OLEDs. LECs have been tested at constant bias, and OLEDs are typically tested at constant current. In constant-current mode, the device brightness is directly proportional to the QE, so the time to go to half-brightness is a good estimate of the half-life of the device. When the LEC is held at a constant bias, the brightness and QE evolve, somewhat independently. The EQE increases over time, as illustrated in Figure 8; however, the current at constant bias decreases over time (Figure 9), so the device brightness at a given bias may actually decrease even though the EQE is increasing. When we tried to evaluate the lifetimes of LECs prepared with **2** at constant

(38) Segal, M.; Baldo, M. A.; Holmes, R. J.; Forrest, S. R.; Soos, Z. G. *Phys. Rev. B* **2003**, *68* (7), 075211−075214.

(39) He, G.; Pfeiffer, M.; Leo, K.; Hofmann, M.; Birnstock, J.; Pudzich, R.; Salbeck, J. *Appl. Phys. Lett.* **2004**, *85*, 3911−3913.

(40) Parker, S. T.; Slinker, J. D.; Lowry, M. S.; Cox, M. P.; Bernhard, S.; Malliaras, G. G. *Chem. Mater.* **2005**, *17*, 3187−3190.

(41) (a) Maness, K. M.; Terrill, R. H.; Meyer, T. J.; Murray, R. W.; Wightman, R. M. *J. Am. Chem. Soc.* **1996**, *118*, 10609−10616. (b) Maness, K. M.; Masui, H.; Wightman, R. M.; Murray, R. W. *J. Am. Chem. Soc.* **1997**, *118*, 3987−3993.

current (after first prebiasing to form the p−n junction), the device was not stable toward loss of the p−n junction. The formation/loss of the p−n junction makes lifetime measurements for LECs a problem. This problem could be eliminated by immobilizing the counterions after the formation of the p−n junction. We are currently examining methods to positionally stabilize the counterions after the p−n junction is formed, similar to the approaches reported for polymer-based LECs.[5,8−10,42] We believe that continual ion diffusion may be related to the short lifetimes typically observed for LECs. Thus, with "frozen" anion LECs, we will be able to carry out lifetime measurements at constant current, analogous to the methods used for OLEDs.

Conclusion

A series of cationic phenylpyrazole-based iridium diimine complexes have been synthesized and their electrochemical, spectroscopic, and electroluminescent properties examined. By simple modification of either the pyrazolyl or diimine ligands, the electrochemical gap and the energy of the lowest emissive state can be varied over a wide range. The HOMO and LUMO energies in the complexes can be independently altered by simple ligand design. Substitution at the diimine ligand led to reduction potentials spanning 0.53 V, while substitution on the ppz ligand led to complexes whose oxidation potentials spanned 0.63 V. The $(ppz)_2Ir(N\hat{}N)^+$ complexes can be tuned to emit throughout the visible spectrum from a MLLCT state. These materials have high phosphorescence efficiencies, which make them ideal active materials for single-layer LECs. Single-layer LEC devices fabricated with these materials exhibit blue, green, and red EL and have EQEs as high as 7.4%.

Acknowledgment. The authors thank Universal Display Corp. and the Department of Energy for financial support of this work.

Supporting Information Available: UV−vis absorption spectra, 77 K emission spectra, and table of DFT-calculated HOMO−LUMO energies for all of compounds examined here. Also included are tables of crystal data, atomic coordinates, bond distances, bond angles, and anisotropic displacement parameters for $(ppz)_2Ir(^t\text{Bu-bpy})^+PF_6^-$ as well as the corresponding CIF files. This material is available free of charge via the Internet at http://pubs.acs.org.

IC050970T

(42) Gao, J.; Yu, G.; Heeger, A. *J. Appl. Phys. Lett.* **1997**, *71*, 1293−1295.